Chemical Engineering & Processing: Process Intensification 193 (2023) 109558

Contents lists available at ScienceDirect

Chemical Engineering and Processing - Process Intensification

journal homepage: www.elsevier.com/locate/cep

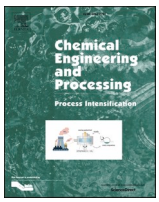

Gas-liquid hydrodynamics of a fractal flow mixer

Muhammad Dary M. Priyambodo [a], Tejas Bhatelia [a,*], Milinkumar Shah [a], Jim Patel [b], Maciej Mazur [c], Vishnu Pareek [a]

[a] WASM: MECE, Curtin University, Bentley, WA 6102, Australia
[b] CSIRO Energy, 71 Normanby Road, Clayton North, Victoria 3169, Australia
[c] RMIT Centre for Additive Manufacturing, School of Engineering, RMIT University, Melbourne, Australia

ARTICLE INFO

Keywords:
Flow distribution
Fractal
High speed imaging
Optical probe
Taylor flow

ABSTRACT

Gas-liquid hydrodynamics of a micro-structured device (fractal flow mixer) was experimentally investigated. Experiments were conducted for a range of liquid-to-gas superficial velocity ratios (V_{SL}/V_{SG}). High-speed imaging was used to identify the flow regimes inside the microchannels of the device at different V_{SL}/V_{SG}. At different V_{SL}/V_{SG}, two or more flow regimes were observed simultaneously in different micro-channels. Consequently, a new flow regime map was developed. An optical probe was used to measure the bubble mean size and velocity. The effect of the V_{SL}/V_{SG} towards the bubble mean size, mean velocity, and frequency were analyzed. The bubble mean size decreases with the increase of the V_{SL}/V_{SG}, which can be attributed to the uniform shearing of gas slugs across all channels. To check the consistency of the fractal flow mixer in producing gas bubbles over a single experiment run, the global relative standard deviation (RSD) was used. The fractal flow mixer was able to generate equal flow distribution across the 16 outlets and maintain a *Taylor* flow over a range of V_{SL}/V_{SG}. . However, depending on the V_{SL}/V_{SG}, the G_B and G_S vary to a certain extent, governed by the capillary effect and the back-pressure.

1. Introduction

Micro-structured channels (including monolithic structures) are characterized by small diffusion paths, high surface-area-to-volume ratio, efficient process control and smaller footprint [1,2], making them highly efficient for heat transfer [3–5] and mass transfer [6–8] applications. It is often assumed that these channels are highly modular and in a multi-channel device, a uniform and controlled inlet fluid flow can be achieved. These inlet devices vary in shape and size depending on the type of application of a micro-structured channel. For example, chamber type [9] and honeycomb designs [7,10,11] have specifically been proposed as microreactors, whereas manifold distributors [12–14] and fractal devices [15–18] have been used as for achieving flow uniformity in heat and mass transfer applications. However, there are very limited large-scale applications of micro-structured channels in the industry, primarily due to the complexity of establishing even and controlled inlet fluid flow in multi-channels.

Table 1 summarizes several studies on multi-channel micro-structured devices designed for different applications. Some of these studies have focused on the design and manufacture aspect, whereas a few studies aimed to characterize either single-phase flow or gas-liquid multiphase flow within the microchannels of the devices. There are different geometries of such devices, that includes fractal, parallel/consecutive, and honeycomb. A fractal design has a sequential design with a low number of divisions per stage but a high number of stages based on self-similar bifurcating channels, while a parallel/consecutive design has a high number of flow divisions per stage [17]. Additionally, a honeycomb design has several divisions in the shape of hexagonal prismatic channels. In the case of single-phase flow through such devices, studies have been conducted to investigate the fluid flow distribution and/or mixing between multiple components. For example, the authors have previously designed and additively manufactured a novel fractal device [17] and tested the flow distribution of the device using a single gas (air). Barbosa et al. [13] proposed a distributor named the *channelCOMB*, a manifold with prismatic channels. To analyze the flow distribution performance, a numerical simulation study with a single gas (air) was carried out to study the effect of the different Reynolds number and geometric parameters. It was found that the main chamber expansion and the length of the outlet channels mainly governs the distribution performance of the device. Barbosa et al. [14] then extended the study to investigate the effect of different additive manufacturing

* Corresponding author.
E-mail address: t.bhatelia@curtin.edu.au (T. Bhatelia).

https://doi.org/10.1016/j.cep.2023.109558
Received 9 June 2023; Received in revised form 5 September 2023; Accepted 22 September 2023
Available online 23 September 2023

Nomenclature

Term	Definition
VP	Vat-photopolymerization
V_{SG}	Gas superficial velocity [m/s]
V_{SL}	Liquid superficial velocity [m/s]
G_S	Gas slugs inside the microchannels
L_S	Liquid slugs inside the microchannels
G_B	gas bubbles dispersing from the outlet of the fractal flow mixer [μm]
BMS	Bubble Mean Size [μm]
BMV	Bubble Mean Velocity [m/s]
d_i	Internal diameter [mm]
RSD	Relative Standard Deviation

techniques towards the flow distribution performance of the *channel-COMB*. It was found that the stereolithography (SLA) technique was better in comparison to fused deposition modelling (FDM) technique due to the better material permeability and fabrication tolerance. Liu et al. [16] and Cao et al. [19] conducted studies using a single-gas (air) to study the effect of fluid properties, channel design (bifurcating stages and angle), operating parameters, and topology optimization. These single-gas multi-channel distributor studies showed that an equal flow distribution can be achieved with different designs, leading to lower pressure losses.

When such devices are used with a multiphase gas-liquid flow, previous studies have focused on flow characterization by defining flow regimes and measuring flow features (local and global) within the microchannels. As shown in Table 1, high-speed imaging, particle image velocimetry, and numerical techniques have been extensively used to understand the gas-liquid hydrodynamics inside multi-channel microstructured devices.

The drag force between the two phases and the contact forces between the phases with the wall at a junction dictate the flow pattern in the microchannel. As a result, inlet flow rates, fluid properties, channel size, channel geometry, and material of construction of the channel are key parameters to optimize the flow inside a microchannel. Several studies have developed flow regime maps based on superficial gas and liquid velocities and have characterized the flow regimes in microchannel as bubbly flow, slug flow or Taylor flow, churn flow, annular flow, and transition flows (i.e. bubbly-slug, churn-annular, etc.) [20–24]. Among these flow patterns, the slug flow or Taylor flow has gained more interest due to its unique feature where elongated, cylindrical gas bubbles occupy the entire cross-sectional area, separated by liquid slugs, and a thin liquid film separates the gas bubbles from the wall of the tube [21,25]. The fluid inside the liquid slug generates recirculation, which induces a higher rate of transport phenomena (mass transfer and heat transfer) [25–27]. Despite its advantages, producing and controlling the Taylor flow within microchannels is rather a challenging task. There are studies that focused on the production of slug flow and investigating its hydrodynamics in a single channel [1,6, 27-29]. Typically, T- junction [23,24,30] or Y- junction [31,32] geometries are used to produce the slug flow in microchannels. However, only a few studies investigated the production and hydrodynamics of Taylor flow in multi-channel bifurcation geometries. As shown in Table 1, Zhang et al. [15] conducted a numerical and an experimental study to provide a theoretical basis to scale up microreactors effectively and to characterize the gas-liquid Taylor flow in a fractal microchannel network with two inlets, four stages of bifurcations, and four outlets. The effect of Reynolds number, the gas-liquid flow rate ratio (j_G/j_L), and the gas inlet direction towards the stability of the Taylor flow, the gas-liquid interface, the flow distribution, and the swirling strength distribution were investigated. Tiwari et al. [33] conducted an experimental study to investigate the hydrodynamics of gas-liquid flow in a T-splitting distributor with two inlets, four stages of bifurcations, and a single outlet. Oil and air were used, and the effect of gas-liquid flow ratio towards the splitting mechanisms, flow regimes, the bubble/slug formation dynamics, and the corresponding relative lengths of bubbles/slugs. Three splitting mechanisms were identified at different gas-liquid flow ratios, including obstructed, partially-obstructed, and non-obstructed. Guo et al. [8] experimentally investigated the effect of different operating parameters and conditions towards the hydrodynamics of a gas-liquid flow in a tree-shaped microchannel. The flow distribution passing through the microchannels was governed by the hydrodynamic feedback effect at the end of branches and the capillary number (Ca) at the T-type bifurcation. Four flow regimes were identified: compact slug flow, slug flow, slug-foam flow, and bubbly foam. Additionally, in order to maintain a high-rate of mass transfer, a critical ratio of gas flow rate to liquid flow rate was determined.

In this work, the authors further extend the previous studies that have been carried out for the fractal flow mixer [17,18] by investigating the hydrodynamics of a gas-liquid flow passing through the fractal flow mixer and also the feasibility of producing Taylor flow within its microchannels. The fractal flow mixer was submerged in a water tank with two inlets of air and water. At first, high-speed imaging (HSI) was used to identify the flow patterns within the microchannels of the fractal flow mixer over a range of air and water inlet flowrate or superficial velocity, which was chosen based on the flow regime map by Triplett et al. [21] to target the slug flow or Taylor flow regime. Once the range of inlet velocities that exclusively produce the Taylor flow regime was identified, an optical probe was used to calculate the bubble size and velocity coming out of each outlet. The flow uniformity across all 16 outlets was analyzed from the optical probe experiment. By tuning the slug size produced, it is expected that the fractal flow mixer can be used for different mass transfer applications while being simultaneously being used as a distributor.

2. Experimental

The fractal flow mixer, as shown in Fig. 1[a], consists of self-bifurcating channels. It was additively manufactured using the vat-photopolymerization (VP) technique with a transparent resin (polymer) precursor. The fractal flow mixer combines the function of a flow distributor and a mixer into a single device. In their prior work, the authors have presented the design and the additive manufacturing process of the fractal flow mixer [17,18]. The geometric parameters of this device are also summarized in Fig. 1[b]. The fractal flow mixer has two inlets or modules with a diameter of 4 mm, which go through four stages of bifurcation. It means that each module is symmetrically bifurcated into a total of 16 channels. These 16 channels from each module were then merged by 16 Y-junctions, resulting in 16 microchannel outlets of 1 mm diameter each. Due to the inherent microchannel geometry of these 16 outlets, it is expected that certain combinations of inlet flow of gas and liquid from the two inlet modules would produce a Taylor flow or a controlled slug flow in the microchannel outlets and produce gas bubbles after the fluid flow is dispersed through the microchannel outlets. In this work, the device was operated using air and water. High-speed imaging was used to observe the gas-liquid flow in the outlet microchannels qualitatively. The combinations of air and water flow rates, which resulted in a Taylor flow in the outlets, were identified. Moreover, the slug sizes were quantified by post-processing the high-speed images and measuring the bubble sizes using an optical probe.

The schematic diagram of the experimental setup is shown in Fig. 2. A custom aluminium frame was used to support the optical probe, lead screw, and the fractal flow mixer. The fractal flow mixer was submerged in a square tank filled with water. The inlet modules were connected to air and water lines. The air and water flow rate were controlled using a mass flow controller and a rotameter. A bypass valve was installed

Table 1
Previous studies on micro- and mili-structured devices with multiple channels.

Authors	Geometry	Application	Manufacturing method and material	Channel size (mm)	Operating parameters		Investigation
					Fluid Properties	Flowrate (mL/min)	
Zhang et al. 2021[*#$]	Fractal[2]	Microreactor	Manufacturing method: template replication method Material: polydimethylsiloxane (PDMS) bonded with polyethylene terephthalate (PET)	0.3 – 2.4	Gas-liquid, Gas: Nitrogen Liquid: Anhydrous ethanol with fluorescent polystyrene tracer particles	0 – 20	(a), (b)
Zou et al. 2021[#^]	Honeycomb[1]	Microreactor	Manufacturing method: Stereo lithography (SLA) Material: photosensitive resin model VisiJet SL Clear	3.7	Liquid-liquid Castor Oil and deionized water	0.3 – 5.4	(a), (b)
Guo et al. 2019[#^]	Fractal[1]	Microreactor	Material: polymethyl methacrylate (PMMA)	0.4	Gas-liquid Gas: CO2 Liquid: 2-amino-2-methyl-1-propanol	Gas to liquid flowrate ratio = 12	(b), (c), (d)
Jiang et al. 2022[*$]	Honeycomb[1]	Microreactor	Manufacturing method: template replication method Material: polydimethylsiloxane (PDMS) bonded with polyethylene terephthalate (PET)	1	Gas-liquid, Gas: Nitrogen Liquid: Deionized water with tracer particles	0 – 10	(a), (c)
Zhang et al. 2018[&$]	Honeycomb[1]	Microreactor	Manufacturing method: SLA 3D printing Material: Transparent resin	2 – 3	Gas-liquid, Gas: CO2 and N2 mixture Liquid: MEA solution	Gas: 40 – 80 Liquid: 5 – 20	(b), (c), (d)
Tiwari et al. 2019[#]	Fractal[1]	Microreactor	Material: PMMA	1 – 2	Gas-liquid Gas: Air Liquid: Oil (Kerosene)	Gas: 3 Liquid: 3 – 16	(a)
Ma et al. 2023*	Honeycomb[1]	Microreactor	Manufacturing method: Precision milling Material: PMMA	0.4 – 0.8	Gas-liquid Gas: CO2 Liquid: IL 1(3-aminopropyl)−3-methyl-imidazolium tetrafluoroborate	Gas-to-liquid flow ratio: 34	(b), (c), (d)
Dong, Xu, and Xu 2017[$]	Fractal[2]	Modular manifold for a fuel cell stack	-	3.2 (outlet) – 8.0 mm	Gas (single) Air	24,000 – 54,400	(c), (e)
Cao et al. 2018[$]	Fractal[2]	Fluid flow distributor	-	Inlet: 16 Outlet: 1	Liquid (single) Water	~ 120.64 – 1206.4	(c), (e)
Liu et al. 2011[&]	Fractal[2]	Fluid flow distributor	Manufacturing method: CNC Material: Plexiglass	Inlet: 4.52 Outlet: 0.77	Gas (single) Air	~18,833.33 – 94,333.33	(c), (e)
Liu, Li, Wang 2012[$]	Fractal[2]	Fluid flow distributor	-	Inlet: 4.52 Outlet: 3.48	Gas (single) Air	~77,020 – 962,760	(c), (e)
Barbosa et al 2021 and 2023[$&]	Parallel/ consecutive[2]	Mesostructured reactor	Manufacturing method: Stereolithography (SLA) and fused deposition modelling (FDM) Material: PLA filament (FDM) and Clear V4 from Formlabs (SLA)	Outlet: 0.994 – 1.036	Gas (single) Air	~54.3 – 136.47	(c), (f)
Priyambodo et al. 2022[$]	Fractal[2]	Fluid flow distributor	Manufacturing method: Vat-photopolymerization (VP) and laser powder bed fusion (L-PBF) Material: Transparent resin (polymer) precursor and Ti-6Al-4V alloy	Inlet: 4 Outlet: 1	Gas Air and Methane	~27.710 – 27,710	(c), (f)
Mazur et al 2019[$&]	Fractal[2]	Fluid flow distributor	Manufacturing method: Vat-photopolymerization (VP) and laser powder bed fusion (L-PBF) Material: Transparent resin (polymer) precursor and Ti-6Al-4V alloy	Inlet: 4 Outlet: 1	Gas (single-phase) Air	~2771 – 27,710	(c), (f)

Type of Study:
* μ-PIV experiment
# Camera or High-speed imaging experiment
^ Numerical
$ CFD
& experiment

Type of outlet:
(1) Single
(2) Multiple

Investigations:
(a) Taylor flow hydrodynamics
(b) Fluid flow hydrodynamics
(c) Flow uniformity
(d) Mass transfer performance
(e) Channel design
(f) Manufacturing method

Inlet diameter	4mm
Outlet diameter	1mm
Number of stages	4
Number of outlets per module	16
Number of mixed channels	16
Y-junction angle	60°

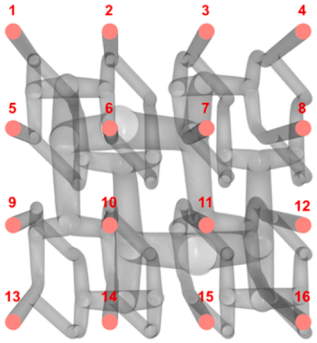

[a] [b] [c]

Fig. 1. [a] The additively manufactured fractal flow mixer, [b] its geometrical parameters, and the [c] Outlet ID.

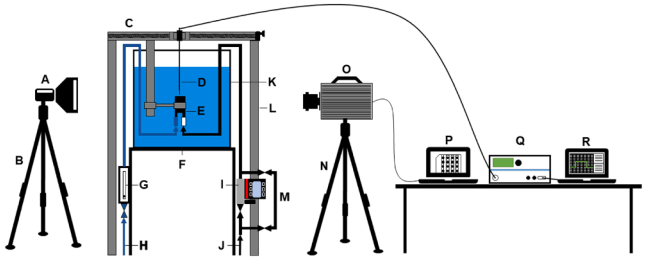

Fig. 2. Schematic diagram of experiment setup [A] LED Light [B] Light stand [C] Lead Screw [D] Optical probe [E] Fractal flow device [F] Metal stand [G] Water rotameter [H] Water inlet [I] Air mass flow controller [J] Air inlet [K] Water tank [L] Custom aluminium frame [M] Bypass valve [N] Camera tripod [O] High-speed camera [P] Laptop 1 (for HSI) [Q] Optoelectronic module [R] Laptop 2 (For optical probe).

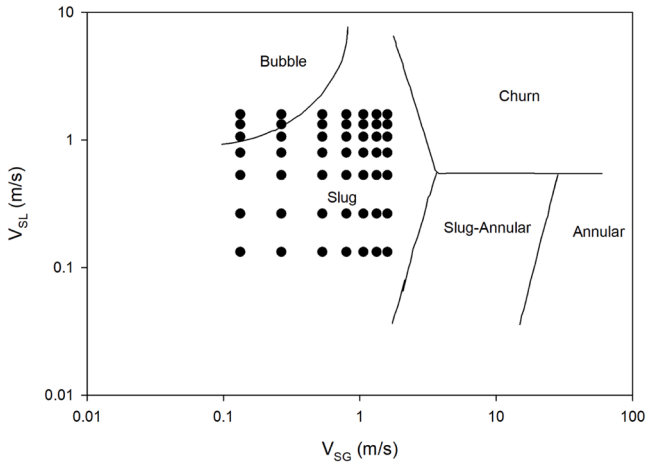

Fig. 3. Regime map for a gas-liquid in a circular micro-channel (di = 1.097 mm) (Triplett et al. 1998) with dots representing tested flow conditions in the current study.

around the air mass flow controller to avoid the channels being flooded with water, especially the air line. In this study, the gas and liquid slugs inside the microchannels will be referred to as G_S and L_S, respectively. Additionally, the gas bubbles dispersing from the outlet of the fractal flow mixer will be referred to as G_B.

The Photron FASTCAM SA4 high-speed camera with a Sigma 105 mm f/2.8 EX DG macro lens was used to capture high-speed images of the fluid flow passing through the microchannels of the fractal flow

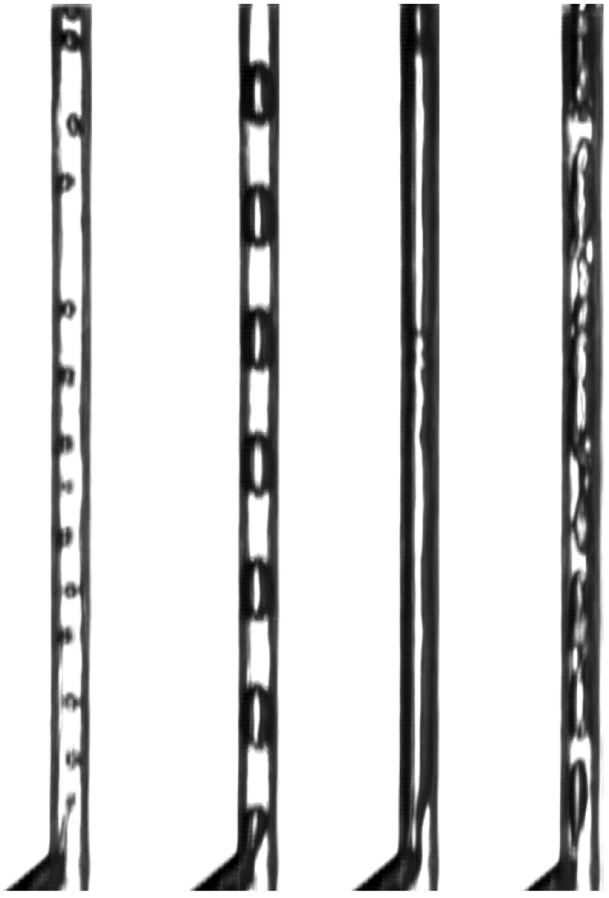

Fig. 4. Identified distinctive flow regimes from the high-speed imaging experiments [a] Bubbly flow [b] Slug flow [c] Annular flow [d] Churn flow.

mixer. The high-speed camera was placed perpendicular to the four visible outlets, and an LED video light was used for illumination. Images were recorded for 0.5 s at 5000 frames per second with a shutter speed of 1/25000s.

The range of inlet flow rates of both water and air for the experiments conducted in this study was selected based on the flow regime map of Triplett 1998 [21], as shown in Fig. 3. The regime map was deduced for a gas-liquid flow in a single circular microchannel with an internal diameter of 1.097 mm. The regime map represented a wide range of gas

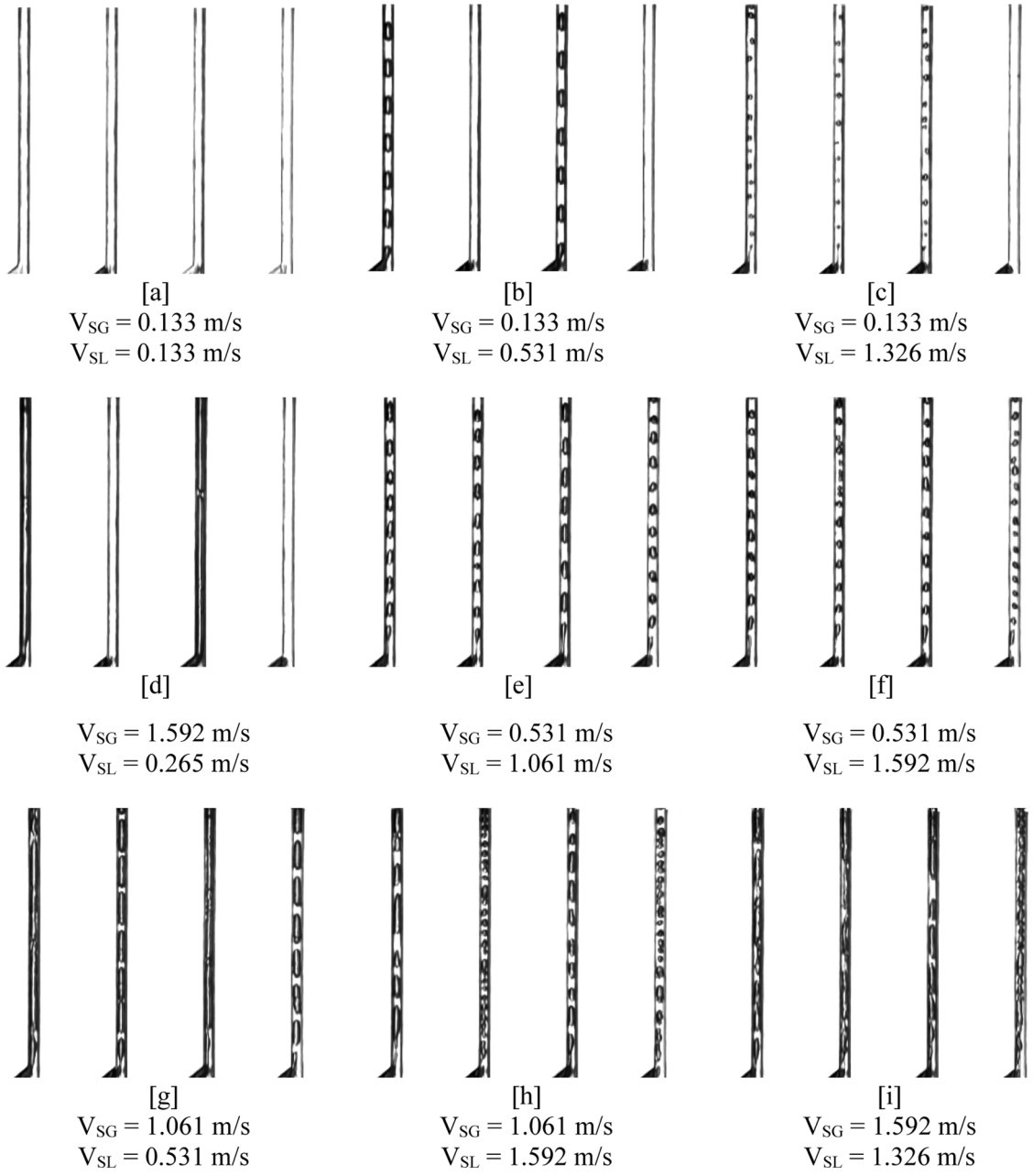

Fig. 5. High-speed imaging experiment results of flow pattern combinations in the front four tubes of the fractal flow mixer (d = 1.00 mm): [a] low flow, [b] low flow and slug flow, [c] low flow and bubbly flow, [d] low flow and annular flow, [e] slug flow, [f] slug and bubbly flow, [g] slug and annular flow, [h] slug and churn flow, [i] churn flow.

superficial velocity (V_{SG}) and liquid superficial velocity (V_{SL}) on the X-axis and Y-axis, respectively. The region on the map was divided into different flow types, including slug flow, slug-annular flow, annular flow, bubbly flow, and churn flow. As the current experimental study intended to produce a slug flow or Taylor flow in the microchannels of the fractal flow mixer, a range of V_{SG} and V_{SL} was selected that was within the slug flow region, as denoted by circular symbols in Fig. 3. The selected range of V_{SG} and V_{SL} was then converted accordingly to the corresponding combinations inlet gas and liquid flowrate for the experiment.

It is important to note that, theoretically, the fractal flow mixer was designed to maintain the same velocity at the inlet and on each outlet tube. Although the tube size is reduced from 4 mm at the inlet to 1 mm at the outlet tubes, the fluid flow is divided into 16 outlet tubes, maintaining the same superficial velocity between each inlet module and the outlet channels. Hence, the inlet velocity or the superficial velocity in the microchannels of air and water will be referred to as the V_{SG} and V_{SL}, respectively. In addition to high-speed imaging, the slug size in the outlet microchannel was measured by characterising the G_B size coming out from each outlet. For this, an optical probe was placed 0.5 cm above an outlet. To measure G_B from 16 different outlets of the fractal flow mixer using the optical probe, the position of the optical probe was changed by operating a lead screw, as shown in Fig. 2. Each outlet was accordingly labelled, as shown in Fig. 1[c].

The optical probe used in this work was a custom-made, single-tip, straight Doppler probe, along with a data acquisition system consisting of an optoelectronic module and post-processing software supplied by A2 Photonic Sensors. The construction and working principle of this optical probe was described in studies previously conducted by Prakash et al. [34,35]. The data acquisition system utilizes a block system to

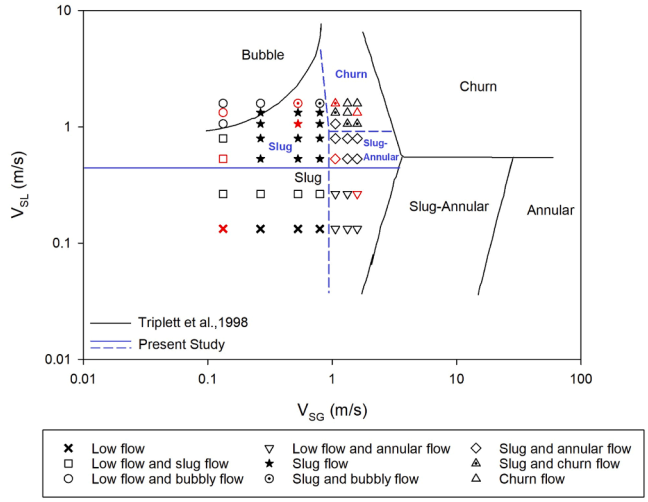

Fig. 6. Identified flow patterns in the outlet channels (d_i = 1.000 mm) of the fractal flow device plotted against the flow regime map by Triplett et al. 1998 [21] for a single circular channel (d_i = 1.097 mm). The solid black lines correspond to flow regime transition lines by Triplett et al. 1998 [21] and the dashed and solid blue lines correspond to flow regime transition lines from this study.

capture invalid and valid gas bubble events. A block independence test was conducted at a V_{SG} of 0.531 m/s and a V_{SL} of 1.061 m/s to determine the optimum number of blocks. Three blocks were tested, that includes 1000, 2000, and 3000 blocks. From the three blocks tested, it was found that the difference in the averaged value (from 3 runs) of Bubble Mean Size (BMS) and Bubble Mean Velocity (BMV) between 2000 blocks and 3000 blocks was 0.69 % and 2.33 %, respectively. Hence, 2000 blocks were chosen for each experiment run conducted in this study. Depending on the velocity tested, on average, 2000 blocks equals ~ 2150 G_B. At a lower velocity (i.e. V_{SG} = 0.265 m/s and V_{SL} = 0.531 m/s), it would be equal to 100–200 G_B and at a higher velocity (i.e. V_{SG} = 0.796 m/s and V_{SL} = 1.326 m/s), it would be equal to 6800 G_B. The experiment was conducted at least in triplicate for each combination of water and air inlet velocities at each outlet tube, totalling 6000 blocks per velocity tested. At lower velocity (i.e. V_{SG} = 0.265 m/s and V_{SL} = 0.531 m/s), it was repeated 5 to 6 times to capture at least 200 G_B in total. Since the block-based system was used in these experiments, the time to complete the pre-determined blocks (2000 blocks) varies from one experiment to another.

3. Results and discussion

3.1. Flow regimes

Initially, HSIs of gas-liquid flow in the front four outlet channels at different gas and liquid operating flow rates were analyzed. The HSI method can only be used to identify the flow patterns in the external outlet channels of the fractal flow mixer. A full tomography must be conducted to qualitatively identify the flow regime of four internal outlet channels of the fractal flow mixer, which is not in the current scope of the study.

Out of 49 gas and liquid flow rate combinations, the images with distinct flow regimes are shown in Fig. 4[a-d]. Four different types of flow regimes were identified: bubbly flow, slug flow, annular flow, and churn flow. Bubbly flow was identified at a high liquid-to-gas ratio of the superficial velocity (low void fraction) (i.e. V_{SG} = 0.133 m/s and V_{SL} = 1.326 m/s). It is a flow regime where the gas phase is distributed in the tube as dispersed non-spherical bubbles that are smaller in diameter than the diameter of the channel. If the V_{SG} is increased, the slug flow was identified (i.e. V_{SG} = 0.531 m/s and V_{SL} = 0.796 m/s). The slug flow is a flow regime where elongated cylindrical gas slugs, also known as Taylor bubbles, occupy almost the entire cross-sectional area of the channel. A thin liquid film separates the gas slugs from the wall of the channel, and a liquid slug exists between the gas slugs. If the ratio of the superficial velocity was swapped, where the V_{SG} is significantly higher than the V_{SL} (high void fraction) (i.e. V_{SG} = 1.061 m/s and V_{SL} = 0.531 m/s), the annular flow was identified. The annular flow is a flow regime that occurs when the gas phase was seen travelling at the center of the channel as a continuous phase with a thin liquid film separating the gas phase from the wall of the channel. The churn flow was observed at an increased volumetric flux of the mixture (V_{SG} + V_{SL}) (i.e. V_{SG} = 1.592 m/s and V_{SL} = 1.326 m/s). The churn flow is a flow regime that occurs when the Taylor gas bubbles deteriorates at higher flowrates due to the transition of a continuous liquid phase into a continuous gas phase.

Furthermore, at different combinations of velocities, two or more flow patterns (low flow, annular flow, slug flow and churn flow) were observed simultaneously in different outlet microchannels of the fractal flow mixer. Hence, a specific range of V_{SG} and V_{SL} is not exclusively

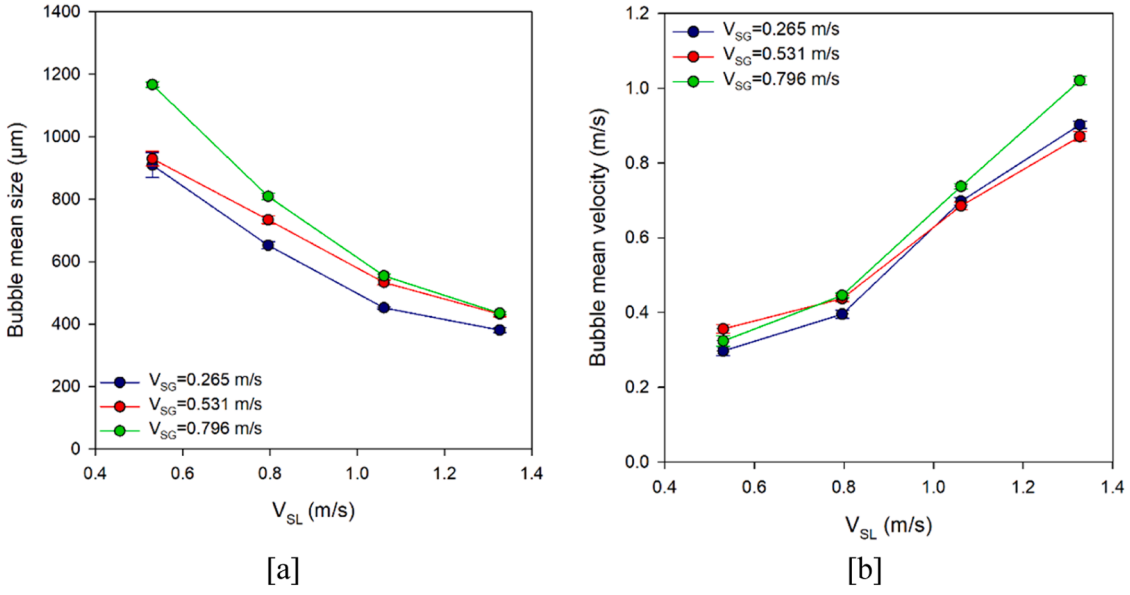

Fig. 7. Global average of [a] bubble mean size and [b] bubble mean velocity across all 16 outlets against V_{SL} at different V_{SG}.

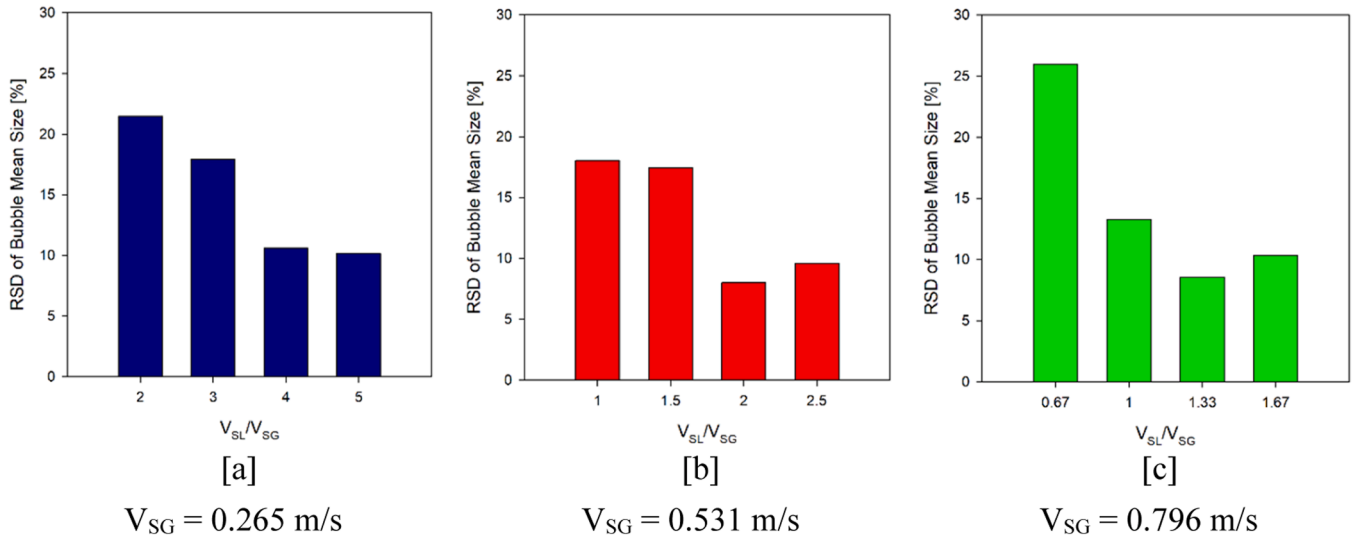

Fig. 8. RSD of bubble mean size across all 16 outlets.

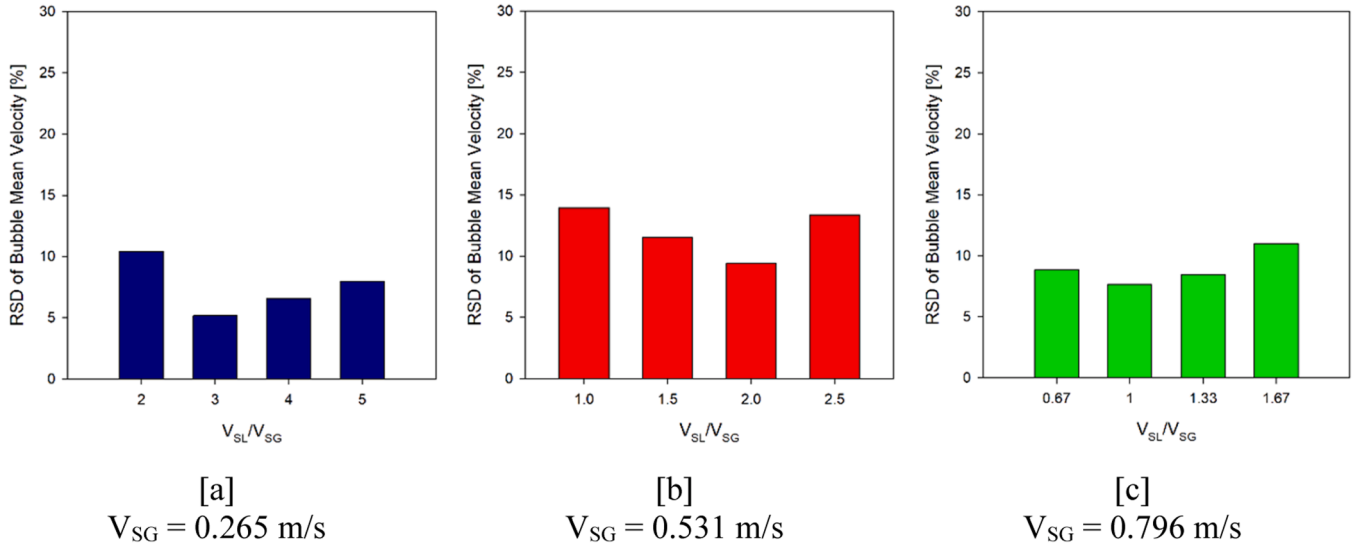

Fig. 9. RSD of bubble mean velocity across all 16 outlets.

related to a particular flow regime, with the exception of the slug flow regime. Starting from the lower V_{SG} and V_{SL} (i.e. V_{SG} = 0.133 m/s and V_{SL} = 0.133 m/s), *low flow* (Fig. 5[a]) was identified. The *low flow* occurs when the V_{SG} is too low to overcome the pressure head in the water tank. Gas slugs are occasionally seen in 1 or 2 channels at this flow regime. Increasing the V_{SG} yet maintaining the V_{SL} (i.e. V_{SG} = 0.133 m/s and V_{SL} = 0.531 m/s), generated the *low flow and slug flow regime* (Fig. 5[b]). Gas slugs were identified in several tubes at this flow regime, while the other tubes were still in the *low flow* regime. Further increase of the V_{SL} (i.e. V_{SG} = 0.133 m/s and V_{SL} = 1.326 m/s) led to a lower void fraction, resulting in the *low flow and bubbly flow* regime (Fig. 5[c]). On the other hand, at a condition where the V_{SG} was significantly higher than the V_{SL} (i.e. V_{SG} = 1.592 m/s and V_{SL} = 0.265 m/s), the *low flow and annular flow* (Fig. 5[d]) was identified. At an increased volumetric flux of the mixture (V_{SG} + V_{SL}) and at a specific combination of V_{SG} and V_{SL} range (i.e. V_{SG} = 0.265 – 0.796 m/s and V_{SL} = 0.535 – 1.326 m/s), the *slug flow* (Fig. 5[e]) was identified. At higher V_{SL}, beyond the range of *slug flow* regime, yet maintaining the V_{SG} within the range of the slug flow regime (i.e. V_{SG} = 0.531 m/s and V_{SL} = 1.592 m/s), resulted in the *slug and bubbly flow* (Fig. 5[f]), where either gas slugs or bubbles were identified across the four tubes. On the other hand, increasing the V_{SG} beyond the range of the *slug flow* regime, yet maintaining the V_{SL} within the range of the slug flow regime (i.e. V_{SG} = 1.061 m/s and V_{SL} = 0.531 m/s), resulted in the *slug and annular flow* (Fig. 5[g]), where either gas slugs or an annular gas flow were identified across the four tubes. At the highest range of mixture volumetric flux tested (i.e. V_{SG} = 1.592 m/s and V_{SL} = 1.326 m/s), the fluid flow fully transitions into a *churn flow* (Fig. 5[i]) across all four tubes.

Fig. 6 shows the observed flow patterns in this study plotted against the flow regime map by Triplett et al. 1998 [21] for a single circular channel (di = 1.097 mm). The experiment conducted by Triplett et al. 1998 [21] had two inlets with a T-junction to mix the two phases of air and water into a single channel/tube. On the other hand, the present study had two inlets, four stages of bifurcation, a Y-junction, and 16 outlet channels/tubes. Another difference between the two studies would be the material of construction of the microchannels, where the study by Triplett et al. 1998 [21] used a Pyrex circular channel (Ace Glass Pyrex Part No. 7740), while the fractal flow mixer presented in this study was additively manufactured using a transparent resin (polymer) precursor. The difference in the surface roughness between the two

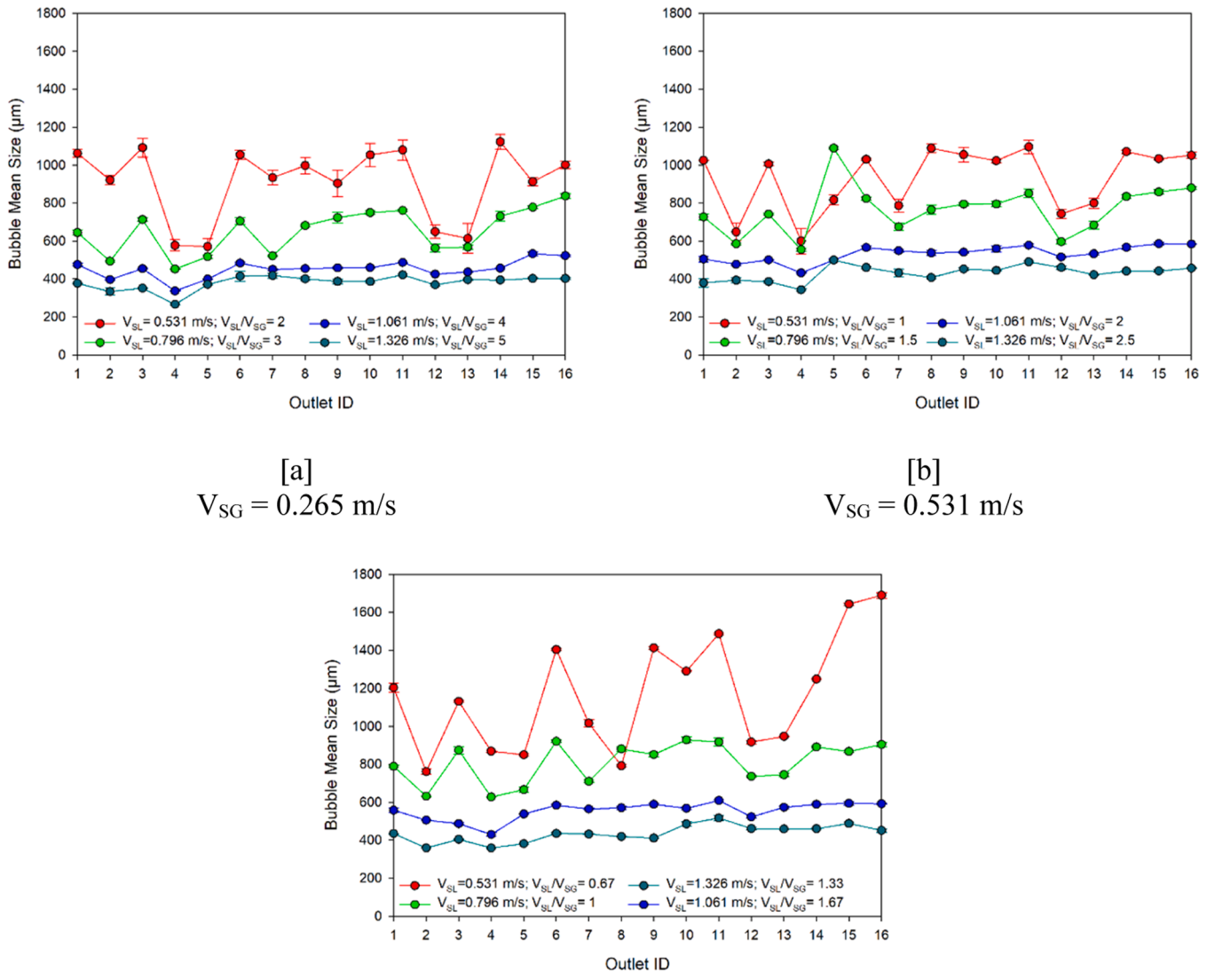

Fig. 10. Bubble mean size at each outlet for [a] V_{SG} = 0.265 m/s [b] V_{SG} = 0.531 m/s [c] V_{SG} = 0.796 m/s.

studies would also contribute to the generated flow regime map. Additionally, from Fig. 6, the scalability of the existing single-channel regime map to be used for multiple channels was observed. It was found that the range of V_{SG} and V_{SL} to produce the slug flow regime has decreased. There is also a shift in the transition lines between the churn flow and the slug-annular flow, starting at a lower value of V_{SL} (i.e. V_{SL} = 1), shown by the dashed blue lines in Fig. 6. Additionally, in order to maintain the presence of G_S in the microchannels, a minimum threshold value was identified for V_{SL}, which is >0.531 m/s. Consequently, a new flow regime map and transition lines (solid and dashed blue lines in Fig. 6) was developed for the fractal flow mixer, which is a device with multiple outlet channels. It must be noted that the current flow regime map is only valid for a specific design of a fractal flow mixer that was presented in this study, which was additively manufactured using the vat-photopolymerization (VP) technique with a transparent resin (polymer) precursor. Different additive manufacturing techniques and materials would result in the microchannel walls of the fractal flow mixer to have a different wetting properties, surface roughness, and friction, affecting the generated divisions of flow regimes from the fractal flow mixer.

3.2. Bubble hydrodynamics

The results from the optical probe experiment that measures the BMS and BMV of the gas bubbles G_B dispersing from the outlet of the fractal flow mixer were further analyzed in this section. The optical probe experiment was conducted over the range of V_{SG} and V_{SL} that exclusively produce slug flow (V_{SG} = 0.265 – 0.796 m/s and V_{SL} = 0.531 – 1.326 m/s). The term *averaged* used in this section refers to the average value from three experiment runs of the optical probe experiment. Meanwhile, the term *global average* refers to the average result from the 16 outlet channels combined. Fig. 7 [a-b] shows the global of the BMS and BMV against the V_{SL} at different V_{SG}. From Fig. 7[a], the global average of BMS decreased with the increase of V_{SL}. This phenomenon occurred at all V_{SG} tested. Furthermore, at all V_{SG} tested, the global average of BMS decreased by ~54 % when the V_{SL} was increased from 0.531 m/s to 1.326 m/s. For the global average of BMV, as shown in Fig. 7[b], the global average of BMV increased by ~244 % when the V_{SL} was increased

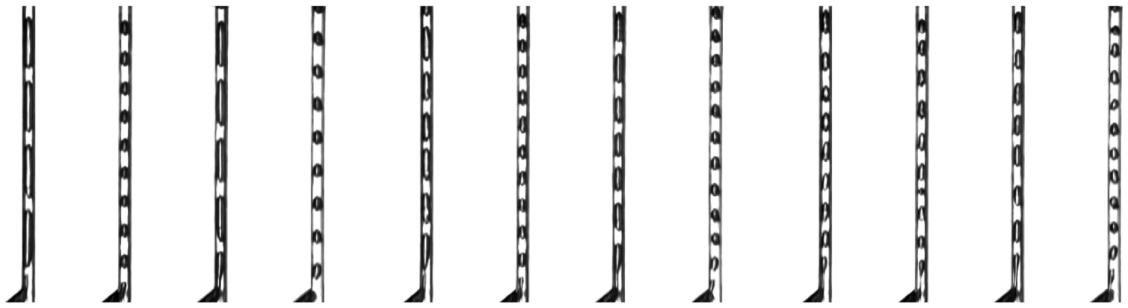

[a] [b] [c]

V_{SG} = 0.531 m/s, V_{SL} = 0.531 m/s, V_{SL}/V_{SG} = 1
V_{SG} = 0.531 m/s, V_{SL} = 0.796 m/s, V_{SL}/V_{SG} = 1.5
V_{SG} = 0.531 m/s, V_{SL} = 1.061 m/s, V_{SL}/V_{SG} = 2

Fig. 11. High-speed imaging experiment results at different V_{SL}/V_{SG}: [a] V_{SL}/V_{SG} = 1; [b] V_{SL}/V_{SG} = 1.5; [c] V_{SL}/V_{SG} = 2.

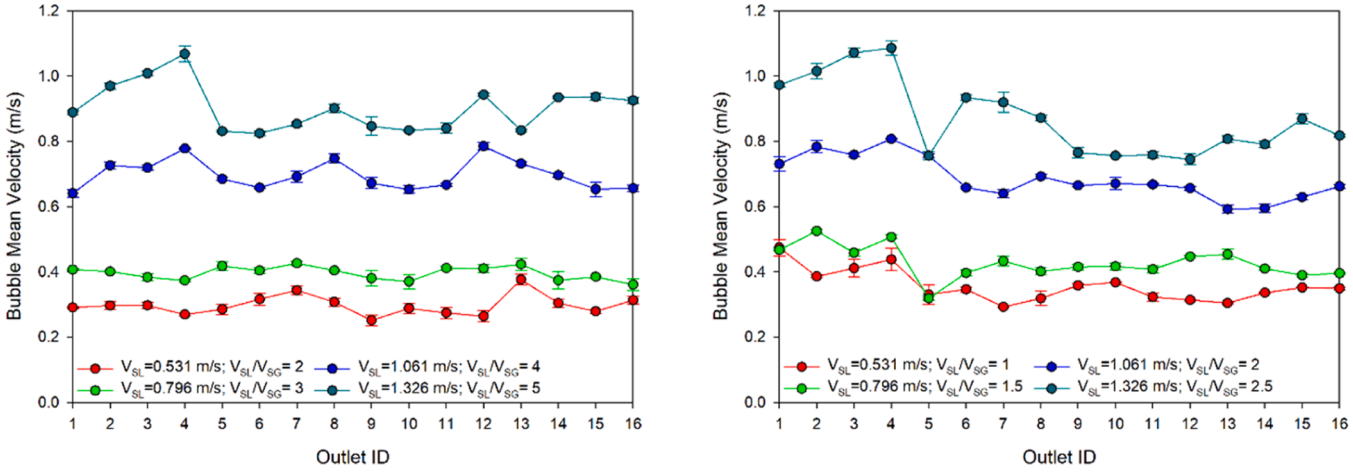

[a] V_{SG} = 0.265 m/s

[b] V_{SG} = 0.531 m/s

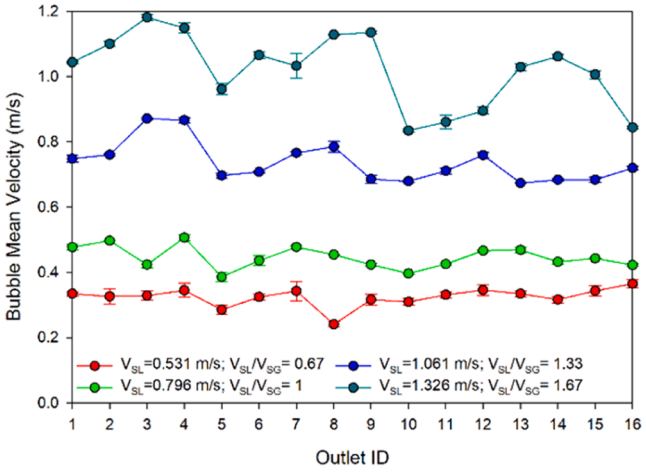

[c] V_{SG} = 0.796 m/s

Fig. 12. Averaged bubble mean velocity at each outlet for (a) V_{SG} = 0.265 m/s (b) V_{SG} = 0.531 m/s (c) V_{SG} = 0.796 m/s.

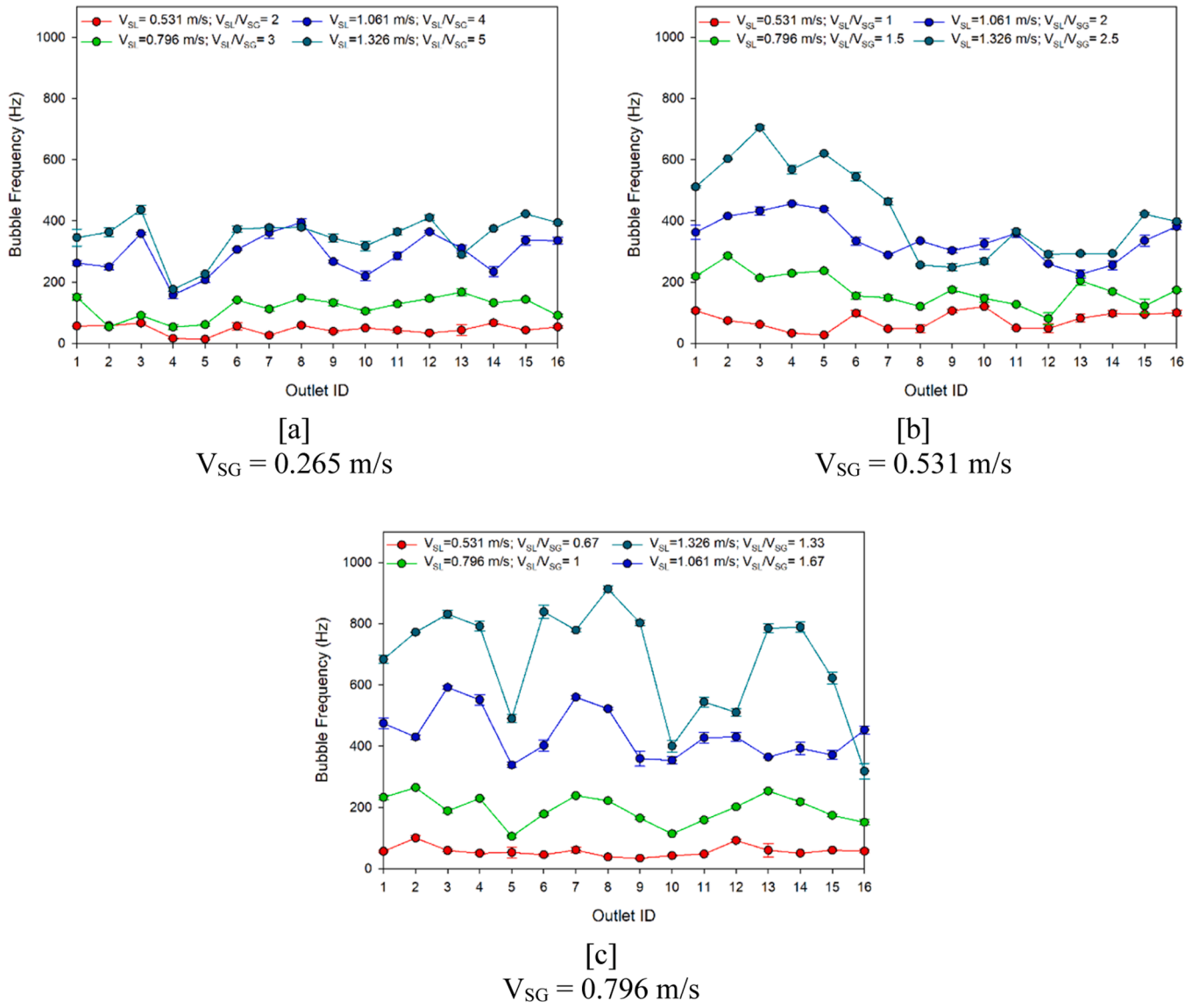

Fig. 13. Bubble frequency at each outlet for [a] V_{SG} = 0.265 m/s [b] V_{SG} = 0.531 m/s [c] V_{SG} = 0.796 m/s.

from 0.531 m/s to 1.326 m/s.

Fig. 8[a-c] shows the global average of the Relative Standard Deviation (RSD) of the BMS. It can be seen that the RSD decreases with the increase of the liquid-to-gas superficial velocity ratio (V_{SL}/V_{SG}). This phenomenon can be attributed to the constant shearing of G_S inside the channels due to the liquid build-up in the channels that occur at a higher V_{SL}/V_{SG}. At a lower V_{SL} and lower V_{SL}/V_{SG}, the kinetic energy in the liquid balances out the capillary force required for shearing the G_S, which is also why the consistency of the flow over the pre-determined number of blocks (2000 blocks) is better at a higher V_{SL}/V_{SG}.

Additionally, the reason of the non-uniformity across the sixteen channels could be due to the fact that the topology of the device is not highly symmetrical. Even though the design philosophy of the device is inherently symmetrical, the distribution of the gas and the liquid can be affected by the upstream velocity pathlines prior to the mixing point. Fig. 9[a-c] shows the global average RSD of BMV across all 16 outlets. For all V_{SG} and V_{SL} tested, the RSD is relatively low (i.e. 5 – 10 %), showing that the fractal flow mixer can provide uniform flow distribution across all sixteen outlet channels.

Figs. 10[a—c] and Figs. 12[a—c] shows the averaged BMS and BMV at each outlet (local average) for different air inlet velocity, respectively. The error bars in Figs. 10[a—c] and Figs. 12[a—c] shows the standard deviation between the three experiment runs conducted for each outlet. From Figs. 10[a—c], as previously shown in Fig. 7[a], the BMS decreases with the increase of the V_{SL}/V_{SG}. Additionally, at lower water inlet velocity (i.e. V_{SL} = 0.531 m/s) and lower ratio of liquid-to-gas (i.e. 1), the G_B distribution among the 16 outlets is uneven. For example, as shown in Fig. 10[b], at V_{SL} = 0.531 m/s and V_{SG} = 0.531 m/s, the difference in G_B size between the smallest (Position ID = 4) and the largest G_B size (Position ID = 11) is ~58.5 %. At a higher V_{SL} (V_{SL} = 0.531 m/s and V_{SG} = 1.326 m/s), the difference between the smallest (Position ID = 4) and the largest G_B size (Position ID = 5) is ~37.12 %. This phenomenon was also shown in Figs. 8[a—c]. Additionally, the effect of the V_{SL}/V_{SG} towards the size distribution of the of G_S at the front four channels were also qualitatively shown in Fig. 11. Figs. 12[a—c] shows that the bubble mean velocity is relatively constant at lower V_{SL} (i.e. 0.531–0.796 m/s) tested. However, variations exist across the sixteen outlets at higher V_{SG} and V_{SL}, which is caused by the random path of bubbles upon exiting the fractal flow device into the water tank, resulting in the bubbles not piercing the optical probe properly.

The flow distribution performance of the fractal flow mixer in producing G_B was also analyzed using the data of bubble frequency at each outlet at different V_{SG}, as shown in Figs. 13[a—c]. It can be seen that at all V_{SG} tested, the bubble frequency increases with the V_{SL}, which is

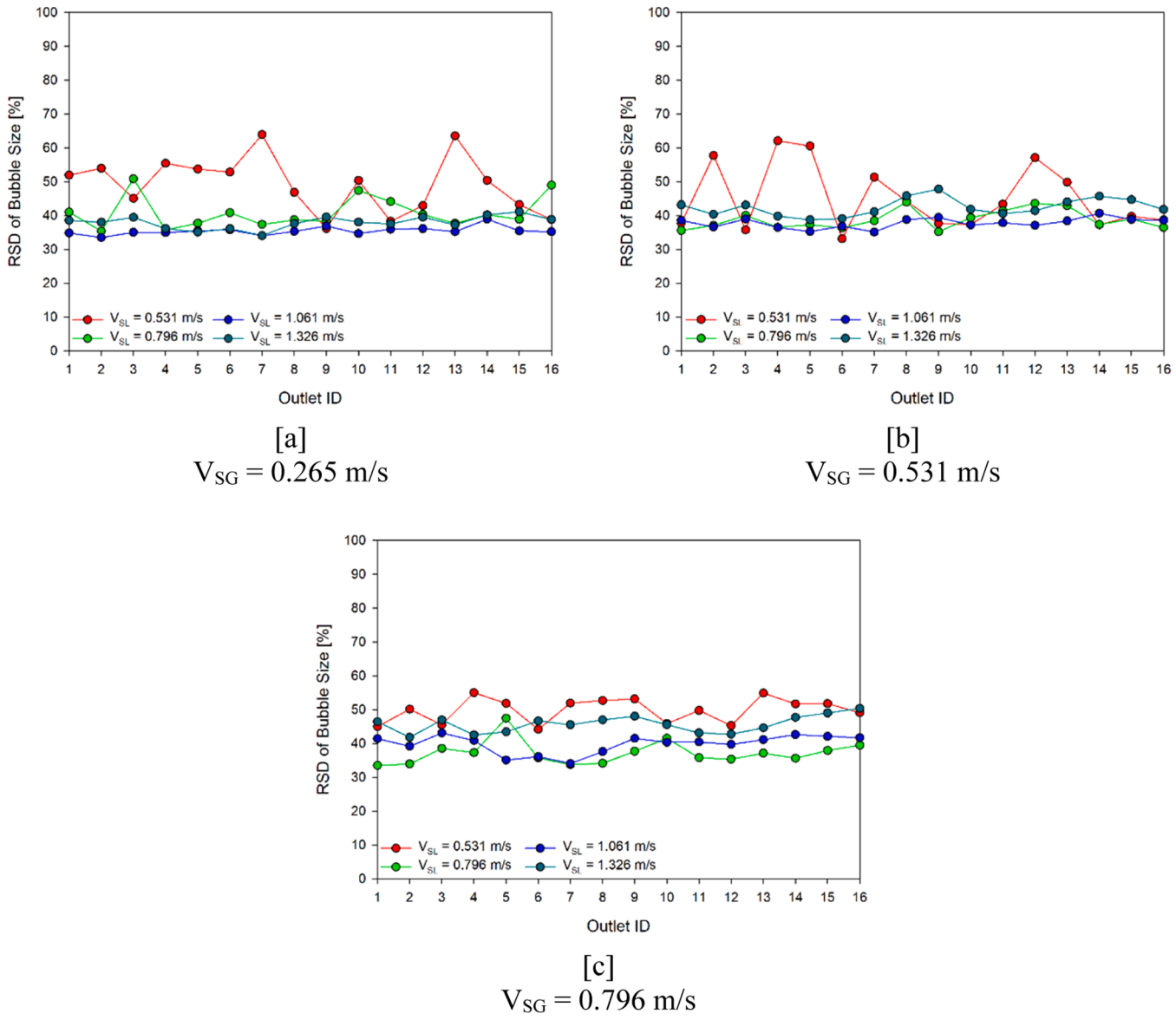

Fig. 14. Relative standard deviation of the bubble size at each outlet for [a] V_{SG} = 0.265 m/s [b] V_{SG} = 0.531 m/s [c] V_{SG} = 0.796 m/s.

expected. The increase of V_{SL} also results in the variation of bubble frequency at different outlets, which is more apparent at higher V_{SG} and V_{SL} (i.e. V_{SG} =0.796 m/s and V_{SL} = 1.326 m/s). Qualitatively, the trend of fluctuation at each outlet between the graphs of bubble mean size (Fig. 10[c]) and the graphs of bubble frequency (Fig. 13[c]) is similar, suggesting that the difference in bubble frequency at each outlet is caused by the difference of bubble size produced at each outlet at higher V_{SG} and V_{SL}.

Besides the use of standard deviation in the form of error bars from the three experiment runs and analysing the bubble frequency, another parameter, the Relative Standard Deviation (RSD), was also used to assess the consistency of the fractal flow mixer in producing G_B at individual outlets (local) over a certain number of blocks (i.e. 2000 blocks). The RSD was calculated based on the total number of bubbles produced on a single experiment run at each outlet, which shows the range of variation of BMS and BMV from the respective average BMS and BMV values at each outlet. The RSD for the size and velocity of the G_B is shown in Figs. 14[a—c] and Figs. 15[a—c], respectively. Both figures shows that the RSD at higher V_{SL} is more consistent (i.e. V_{SL} = 1.061–1.326 m/s) in comparison to lower V_{SL} (i.e. V_{SL} = 0.531–0.796 m/s).

4. Conclusion

In this work, the gas-liquid hydrodynamics of the fractal flow mixer was investigated. High-speed imaging (HSI) was used to identify the flow regimes and to measure the size of the gas slugs generated within the front four microchannels of the device. Four distinctive flow regimes were identified: Bubbly flow, slug flow, annular flow, and churn flow. At different combinations of velocities, two or more flow regimes (low flow, annular flow, slug flow and churn flow) were observed simultaneously in different outlet microchannels, resulting in nine combinations of flow patterns observed across the four channels. In future studies, a full tomography can be done to qualitatively identify the flow regimes on the internal outlet channels.

Furthermore, comparing the identified flow regimes from the HSI experiment conducted against the flow regime map by Triplett et al. 1998 [21] for a single circular channel (d_i = 1.097 mm), it was found that the slug flow regime has decreased in size to a smaller range of V_{SG} and V_{SL}. There is also a shift in the transition lines of the churn and slug-annular flow, that occurs at a lower value of the V_{SL} (i.e. V_{SL} = 1). The shift in transition lines has resulted in the development of a new flow regime map for the fractal flow mixer, which is a device with

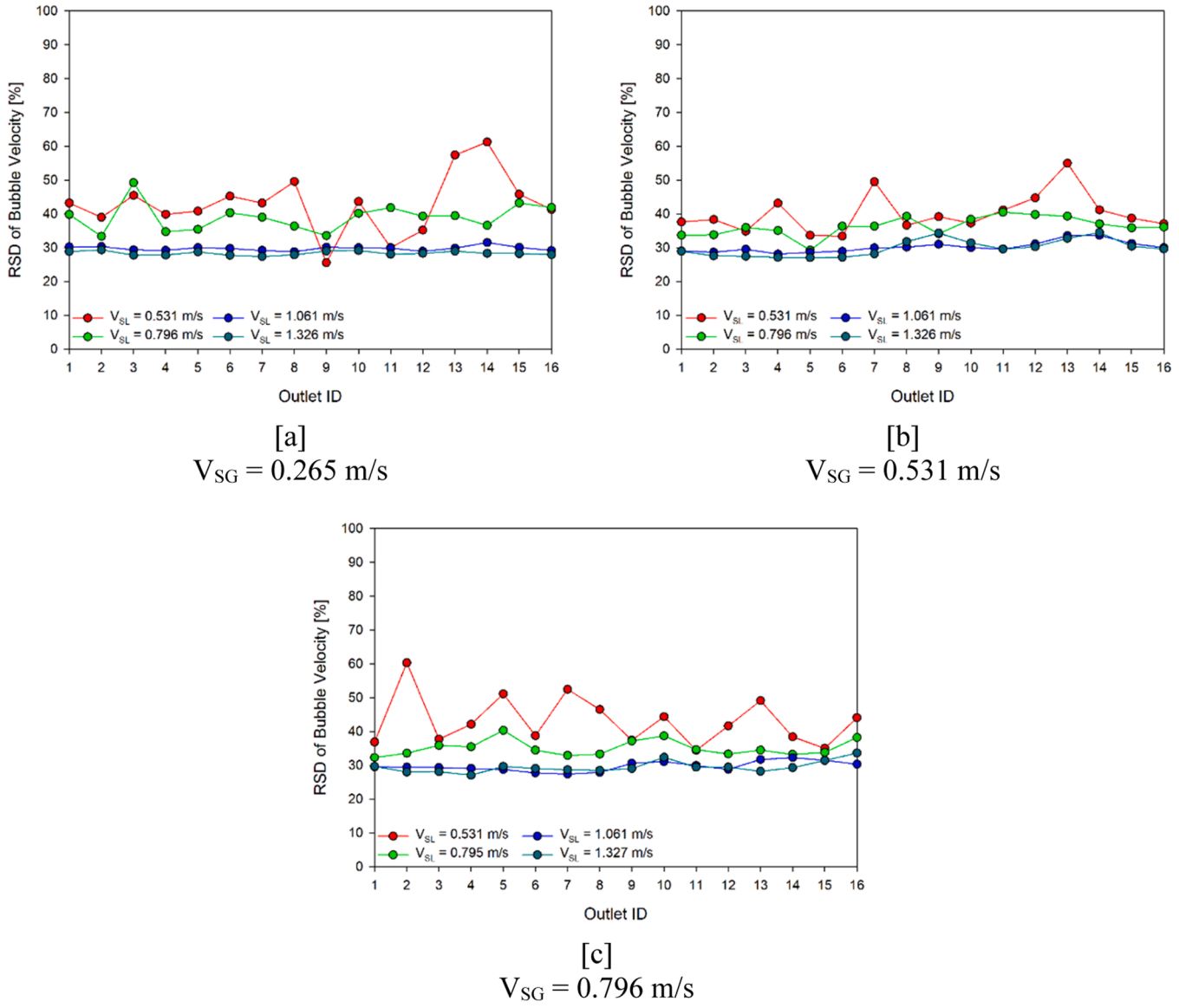

Fig. 15. Relative standard deviation of the bubble velocity at each outlet for [a] V_{SG} = 0.265 m/s [b] V_{SG} = 0.531 m/s [c] V_{SG} = 0.796 m/s.

multiple channels (Fig. 6).

Once the V_{SG} and V_{SL} combinations in the slug flow regime were identified, an optical probe was used to measure the bubble mean size and velocity coming out of each sixteen outlet channels of the fractal flow mixer. The experiment was carried out at different V_{SL}/V_{SG}. From the optical probe experiment, it was concluded that the increase of the V_{SL}/V_{SG} resulted in the decrease of the global average of the BMS and the increase of the global average of the BMV. Similar trends were observed from the averaged BMS and the local BMV within each outlet. From the global average of RSD of the BMS across all 16 outlets, it was found that the RSD decreases with the increase of the V_{SL}/V_{SG}, which can be attributed to the constant shearing of gas slugs due to the liquid build-up in the channels that occur at a higher liquid-to-gas ratio. Looking at the local RSD of bubble size and bubble velocity at each outlet, the RSD is more consistent at higher V_{SL}. Thus, it was concluded that the fractal flow mixer was able to generate an equal flow distribution across the 16 outlets and maintained a Taylor flow over a certain range of V_{SL}/V_{SG}. However, depending on the V_{SL}/V_{SG}, the G_B and G_S vary to a certain extent, governed by the capillary effect and the back-pressure. Additionally, further studies can be conducted on the fractal flow mixer for different applications at different scales. The fractal flow mixer can potentially be used as an aeration device, a burner, a monolith reactor, a flow distributor, etc.

Statement of novelty and significance

The interest in micro-structured devices has increased in recent years for process intensification and chemical synthesis purposes. An example of such device is the fractal flow mixer presented in this study, which is a multi-channel micro-structured flow distribution and mixing device. The effect of the liquid-to-gas superficial velocity ratio (V_{SL}/V_{SG}) was studied. From the high speed imaging experiment, a new flow regime map for the device was developed. Furthermore, the optical probe experiment showed that the fractal flow device was able to generate an equal flow distribution across all outlets and maintain a Taylor flow over a range of V_{SL}/V_{SG}.

Author contribution statement

Muhammad Dary Mahadika Priyambodo: Writing, drafting, result analysis, and reviewing for the simulation modelling part of the study. **Tejas Bhatelia:** Conceptualising, Writing sections, result analysis, and

reviewing. **Milinkumar Shah:** Conceptualising, Writing sections, result analysis, and reviewing. **Jim Patel:** Conceptualising, result analysis, and reviewing. **Maciej Mazur:** Conceptualising, result analysis, and reviewing. **Vishnu Pareek:** Conceptualising, result analysis, and reviewing.

Declaration of Competing Interest

The authors declare that they have no known competing financial interests or personal relationships that could have appeared to influence the work reported in this paper

Data availability

Data will be made available on request.

Acknowledgments

All authors received funding from the Australian Research Council (Project ID: LP160101181).

References

[1] R. Gupta, D.F. Fletcher, B.S. Haynes, On the CFD modelling of Taylor flow in microchannels, Chem. Eng. Sci. 64 (12) (2009) 2941–2950, https://doi.org/10.1016/j.ces.2009.03.018, 2009/06/15/.
[2] K. Jähnisch, V. Hessel, H. Löwe, M. Baerns, Chemistry in microstructured reactors, Angew. Chem. Int. Ed. 43 (4) (2004) 406–446, https://doi.org/10.1002/anie.200300577, 2004/01/16.
[3] M. Ohadi, K. Choo, S. Dessiatoun, E. Cetegen, Emerging Applications of Microchannels, in: Ohadi M., Choo K., Dessiatoun S., Cetegen E. (Eds.), Next Generation Microchannel Heat Exchangers, Springer, New York, 2013, pp. 67–105.
[4] G. Mohiuddin Mala, D. Li, J.D. Dale, Heat transfer and fluid flow in microchannels, Int. J. Heat Mass Transf. 40 (13) (1997) 3079–3088, https://doi.org/10.1016/S0017-9310(96)00356-0, 1997/09/01/.
[5] A.N. Asadolahi, R. Gupta, S.S.Y. Leung, D.F. Fletcher, B.S. Haynes, Validation of a CFD model of Taylor flow hydrodynamics and heat transfer, Chem. Eng. Sci. 69 (1) (2012) 541–552, https://doi.org/10.1016/j.ces.2011.11.017, 2012/02/13/.
[6] R. Abiev, S. Svetlov, S. Haase, Hydrodynamics and mass transfer of gas-liquid and liquid-liquid Taylor flow in microchannels, Chem. Eng. Technol. 40 (11) (2017) 1985–1998, https://doi.org/10.1002/ceat.201700041, 2017/11/01.
[7] D. Ma, G. Wang, Y. Ma, C. Zhu, X. Tang, Hydrodynamics behavior and mass transfer performance of gas–liquid two-phase flow in the honeycomb fractal microreactor, Chem. Eng. J. 462 (2023), 142228, https://doi.org/10.1016/j.cej.2023.142228, 2023/04/15/.
[8] R. Guo, T. Fu, C. Zhu, Y. Yin, Y. Ma, Hydrodynamics and mass transfer of gas-liquid flow in a tree-shaped parallel microchannel with T-type bifurcations, Chem. Eng. J. 373 (2019) 1203–1211, https://doi.org/10.1016/j.cej.2019.05.124, 2019/10/01/.
[9] Z. Dong, Z. Wen, F. Zhao, S. Kuhn, T. Noël, Scale-up of micro- and milli-reactors: an overview of strategies, design principles and applications, Chem. Eng. Sci. X 10 (2021), 100097, https://doi.org/10.1016/j.cesx.2021.100097, 2021/05/01/.
[10] Y. Jiang, Y. Zhang, J. Zhang, and Z. Tang, "Characteristics of gas-liquid slug flow in honeycomb microchannel reactor," Energies, vol. 15, no. 4, doi: 10.3390/en15041465.
[11] S. Zhang, Y. Lu, Y. Gu, X. Zhang, J. Sun, Z. Tang, The process intensification of CO2 absorption in honeycomb fractal reactor fabricated by 3D printer, Chem. Eng. Process. 132 (2018) 42–47, https://doi.org/10.1016/j.cep.2018.08.013, 2018/10/01/.
[12] J. Dong, X. Xu, B. Xu, CFD analysis of a novel modular manifold with multi-stage channels for uniform air distribution in a fuel cell stack, Appl. Therm. Eng. 124 (2017) 286–293, https://doi.org/10.1016/j.applthermaleng.2017.06.030, 2017/09/01/.
[13] I.S.O. Barbosa, R.J. Santos, C.G. Silva, M.S.C.A. Brito, Consecutive flow distributor device for mesostructured reactors and networks of reactors, Chem. Eng. Process. 167 (2021), 108541, https://doi.org/10.1016/j.cep.2021.108541, 2021/10/01/.
[14] I.S.O. Barbosa, et al., ChannelCOMB device for mesostructured reactors and networks of reactors, Chem. Eng. Technol. 46 (6) (2023) 1241–1250, https://doi.org/10.1002/ceat.202200560, 2023/06/01.
[15] Y. Zhang, J. Zhang, Z. Tang, Q. Wu, Gas–liquid taylor flow characteristics in a fractal microchannel network during numbering-up and sizing-up,, Ind. Eng. Chem. Res. 60 (21) (2021) 7935–7949, https://doi.org/10.1021/acs.iecr.1c00448, 2021/06/02.
[16] H. Liu, P. Li, J.V. Lew, D. Juarez-Robles, Experimental study of the flow distribution uniformity in flow distributors having novel flow channel bifurcation structures, Exp. Therm. Fluid Sci. 37 (2012) 142–153, https://doi.org/10.1016/j.expthermflusci.2011.10.015, 2012/02/01/.
[17] M. Mazur, et al., Additively manufactured, highly-uniform flow distributor for process intensification, Chem. Eng. Process. 143 (2019), 107595, https://doi.org/10.1016/j.cep.2019.107595, 2019/09/01/.
[18] M.D.M. Priyambodo, et al., Numerical evaluation of an additively manufactured uniform fractal flow mixer, Chem. Eng. Process. 179 (2022), 109047, https://doi.org/10.1016/j.cep.2022.109047, 2022/09/01/.
[19] J. Cao, M. Kraut, R. Dittmeyer, L. Zhang, H. Xu, Numerical analysis on the effect of bifurcation angle and inlet velocity on the distribution uniformity performance of consecutive bifurcating fluid flow distributors, Int. Commun. Heat Mass Transf. 93 (2018) 60–65, https://doi.org/10.1016/j.icheatmasstransfer.2017.04.017, 2018/04/01/.
[20] K. Mishima, T. Hibiki, Some characteristics of air-water two-phase flow in small diameter vertical tubes, Int. J. Multiph. Flow 22 (4) (1996) 703–712, https://doi.org/10.1016/0301-9322(96)00010-9, 1996/08/01/.
[21] K.A. Triplett, S.M. Ghiaasiaan, S.I. Abdel-Khalik, D.L. Sadowski, Gas–liquid two-phase flow in microchannels Part I: two-phase flow patterns,, Int. J. Multiph. Flow 25 (3) (1999) 377–394, https://doi.org/10.1016/S0301-9322(98)00054-8, 1999/04/01/.
[22] L. Chen, Y.S. Tian, T.G. Karayiannis, The effect of tube diameter on vertical two-phase flow regimes in small tubes, Int. J. Heat Mass Transf. 49 (21) (2006) 4220–4230, https://doi.org/10.1016/j.ijheatmasstransfer.2006.03.025, 2006/10/01/.
[23] J. Yue, G. Chen, Q. Yuan, L. Luo, Y. Gonthier, Hydrodynamics and mass transfer characteristics in gas–liquid flow through a rectangular microchannel, Chem. Eng. Sci. 62 (7) (2007) 2096–2108, https://doi.org/10.1016/j.ces.2006.12.057, 2007/04/01/.
[24] J. Yue, L. Luo, Y. Gonthier, G. Chen, Q. Yuan, An experimental investigation of gas–liquid two-phase flow in single microchannel contactors, Chem. Eng. Sci. 63 (16) (2008) 4189–4202, https://doi.org/10.1016/j.ces.2008.05.032, 2008/08/01/.
[25] T. Abadie, J. Aubin, D. Legendre, C. Xuereb, Hydrodynamics of gas–liquid Taylor flow in rectangular microchannels, Microfluid. Nanofluidics 12 (1) (2012) 355–369, https://doi.org/10.1007/s10404-011-0880-8, 2012/01/01.
[26] S.S.Y. Leung, Y. Liu, D.F. Fletcher, B.S. Haynes, Heat transfer in well-characterized Taylor flow, Chem. Eng. Sci. 65 (24) (2010) 6379–6388, https://doi.org/10.1016/j.ces.2010.09.014, 2010/12/15/.
[27] R. Gupta, D.F. Fletcher, B.S. Haynes, Taylor flow in microchannels: a review of experimental and computational work, J. Comput. Multiph. Flows 2 (1) (2010) 1–31, https://doi.org/10.1260/1757-482X.2.1.1, 2010/03/01.
[28] P. Angeli, A. Gavriilidis, Hydrodynamics of Taylor flow in small channels: a review, Proc. Inst. Mech. Eng. C J. Mech. Eng. Sci. 222 (5) (2008) 737–751, https://doi.org/10.1243/09544062JMES776, 2008/05/01.
[29] A. Etminan, Y.S. Muzychka, K. Pope, A review on the hydrodynamics of Taylor flow in microchannels: experimental and computational studies,, Processes 9 (5) (2021), https://doi.org/10.3390/pr9050870.
[30] H. Liu, Y. Zhang, Droplet formation in a T-shaped microfluidic junction, J. Appl. Phys. 106 (3) (2009), 034906, https://doi.org/10.1063/1.3187831.
[31] L. Lei, Y. Zhao, X. Wang, G. Xin, J. Zhang, Experimental and numerical studies of liquid-liquid slug flows in micro channels with Y-junction inlets, Chem. Eng. Sci. 252 (2022), 117289, https://doi.org/10.1016/j.ces.2021.117289, 2022/04/28/.
[32] A.E. Lim, Y.C. Lam, Vertical squeezing route taylor flow with angled microchannel junctions, Ind. Eng. Chem. Res. 60 (39) (2021) 14307–14317, https://doi.org/10.1021/acs.iecr.1c02324, 2021/10/06.
[33] A. Tiwari, A. Maheshwari, V.M. Rajesh, K.B. Singh, Experimental characterization of gas-liquid flows in splitting distributor for parallel micro-channels, Chem. Eng. J. 377 (2019), 120602, https://doi.org/10.1016/j.cej.2018.12.062, 2019/12/01/.
[34] B. Prakash, M.T. Shah, V.K. Pareek, R.P. Utikar, Impact of HSPBT blade angle on gas phase hydrodynamics in a gas–liquid stirred tank, Chem. Eng. Res. Des. 130 (2018) 219–229, https://doi.org/10.1016/j.cherd.2017.12.028, 2018/02/01/.
[35] B. Prakash, H. Parmar, M.T. Shah, V.K. Pareek, L. Anthony, R.P. Utikar, Simultaneous measurements of two phases using an optical probe, Exp. Comput. Multiph. Flow 1 (4) (2019) 233–241, https://doi.org/10.1007/s42757-019-0025-y, 2019/12/01.